RETRACTION

Post date 9 October 2015

Our Report "Ultrahigh magnetoresistance at room temperature in molecular wires" (*1*) presents measurements on one-dimensional molecular chains confined inside the nanochannels of zeolite L crystals. In these measurements we observed signals that were interpreted as an exceptionally large (~1000%) response of the conductance through the molecular chains to an external magnetic field of a few millitesla. The explanation of the results was based on a room-temperature Pauli spin blockade effect, intrinsic to the hopping transport through the molecules. The observed magnetic field scale of a few millitesla could be explained by the typical magnitude of the random nuclear magnetic field in the molecular environment. The shape of the conductance versus magnetic field dependence was found to be in close agreement with similar curves observed in bulk organic semiconductors, in which the effect is referred to as "organic magnetoresistance" or "OMAR." The exceptionally large effect in our case was ascribed to the one-dimensional nature of electron transport along the molecular chains.

In follow-up research by some of the co-authors, suspicion arose with regard to data collected by the first author Rabindra N. Mahato, which led to a thorough investigation by the co-authors. This investigation has revealed inappropriate data handling by Dr. Mahato, such that the experimental results are not accurately represented in the paper. This makes it, in our eyes, impossible to solidly underpin the conclusions made in the report. All co-authors have therefore concluded that the paper should be immediately retracted. Dr. Mahato has agreed to this Retraction.

R. N. Mahato,[1] H. Lülf,[2] M. H. Siekman,[1,3] S. P. Kersten,[4] P. A. Bobbert,[4] M. P. de Jong,[1] L. De Cola,[2,5] W. G. van der Wiel[1]*

[1]School of Physical Sciences, Jawaharlal Nehru University, New Delhi-110067, India. [2]Institut de Science et d'Ingénierie Supramoléculaires (ISIS), Université de Strasbourg, Strasbourg, 67000, France. [3]Transducers Science and Technology Group, MESA+ Institute for Nanotechnology, University of Twente, Enschede, 7500AE, Netherlands. [4]Molecular Materials and Nanosystems, Department of Applied Physics, Eindhoven University of Technology, Eindhoven, 5600 MB, Netherlands. [5]Karlsruher Institut für Technologie (KIT), Eggenstein-Leopoldshafen, D-76344, Germany.

*Corresponding author. E-mail: w.g.vanderwiel@utwente.nl

Reference

1. R. N. Mahato *et al.*, *Science* **341**, 257 (2013).

patterns decay back to the static seven-droplet pattern within a fraction of a second.

Dynamic patterns rely critically on low friction and energy dissipation (movie S12). The geometry of the dynamic patterns cannot be described in terms of energy minimization (Eq. 2), because they are far from the energy minimum. Instead, the patterns are better described and rationalized as dynamic states wherein the droplet number is kinetically trapped [as in the static patterns (Fig. 2C)]. Patterns can be classified into those that alternate (Fig. 4E) or do not alternate (Fig. 4D) during the cycled energy feed. Alternation is caused by different mobilities of the droplets: Elongated ones are more mobile because of the higher ratio between the driving and dissipative forces.

Dynamic self-assembly can be used as a switch between droplet patterns with different numbers of droplets. In contrast to the division instability, dynamic self-assembly decreases the number of droplets. This allows the irreversibility of the droplet formation in static self-assembly (Fig. 2C) to be overcome. For example, driving any static pattern to the mode V dynamic pattern (single elongated droplet) and decreasing the magnetic field while oscillating the magnet allows recovery of the original one-droplet state (movie S13). This is the final unit operation required to realize a complete cycle from a single liquid droplet to complicated static and dynamic patterns and, finally, back to the starting state (fig. S10).

Externally driven magnetic droplets on superhydrophobic surfaces form a versatile model system for studying and visualizing complicated phenomena in self-assembly. We used this model to demonstrate switching between static and dynamic self-assembly and to show the usefulness of kinetic trapping that most often is viewed only as a hindrance for assembly. The most diverse patterns were found to occur near the boundary where static patterns switch to dynamic ones. The transition is complex, and its detailed investigations will pave the way toward a better understanding of the onset of dynamic dissipative self-assembly.

References and Notes

1. P. Ball, *Nature's Patterns: A Tapestry In Three Parts* (Oxford Univ. Press, Oxford, 2011).
2. G. M. Whitesides, B. Grzybowski, *Science* **295**, 2418–2421 (2002).
3. F. S. Bates *et al*., *Science* **336**, 434–440 (2012).
4. A.-V. Ruzette, L. Leibler, *Nat. Mater.* **4**, 19–31 (2005).
5. Y. Xia *et al*., *Nat. Nanotechnol.* **6**, 580–587 (2011).
6. E. V. Shevchenko, D. V. Talapin, N. A. Kotov, S. O'Brien, C. B. Murray, *Nature* **439**, 55–59 (2006).
7. K. Liu, N. Zhao, E. Kumacheva, *Chem. Soc. Rev.* **40**, 656–671 (2011).
8. T. Kato, N. Mizoshita, K. Kishimoto, *Angew. Chem. Int. Ed.* **45**, 38–68 (2006).
9. O. Ikkala, G. ten Brinke, *Science* **295**, 2407–2409 (2002).
10. S. Park *et al*., *Science* **323**, 1030–1033 (2009).
11. J. Yoon, W. Lee, E. L. Thomas, *MRS Bull.* **30**, 721–726 (2005).
12. B. A. Grzybowski, C. J. Campbell, *Chem. Eng. Sci.* **59**, 1667–1676 (2004).
13. B. A. Grzybowski, C. E. Wilmer, J. Kim, K. P. Browne, K. J. M. Bishop, *Soft Matter* **5**, 1110–1128 (2009).
14. S. Kauffman, *At Home in the Universe: The Search for Laws of Self-Organization and Complexity* (Oxford Univ. Press, Oxford, 1995).
15. E. Karsenti, *Nat. Rev. Mol. Cell Biol.* **9**, 255–262 (2008).
16. A. M. Mateus, N. Gorfinkiel, A. M. Arias, *Semin. Cell Dev. Biol.* **20**, 877–884 (2009).
17. B. A. Grzybowski, H. A. Stone, G. M. Whitesides, *Nature* **405**, 1033–1036 (2000).
18. K. V. Tretiakov, K. J. M. Bishop, B. A. Grzybowski, *Soft Matter* **5**, 1279–1284 (2009).
19. R. E. Rosensweig, *Ferrohydrodynamics* (Dover Publications, New York, 1997).
20. J.-C. Bacri, F. Elias, in *Morphogenesis: Origins of Patterns and Shapes*, P. Bourgine, A. Lesne, Eds. (Springer, Heidelberg, 2011), pp. 15–19.
21. R. Massart, *IEEE Trans. Magn.* **17**, 1247–1248 (1981).
22. W. Barthlott, C. Neinhuis, *Planta* **202**, 1–8 (1997).
23. I. A. Larmour, S. E. J. Bell, G. C. Saunders, *Angew. Chem. Int. Ed.* **46**, 1710–1712 (2007).
24. X. F. Gao *et al*., *Adv. Mater.* **19**, 2213–2217 (2007).
25. H. Mertaniemi *et al*., *Adv. Mater.* **23**, 2911–2914 (2011).
26. H. Mertaniemi, R. Forchheimer, O. Ikkala, R. H. A. Ras, *Adv. Mater.* **24**, 5738–5743 (2012).
27. T. Verho *et al*., *Proc. Natl. Acad. Sci. U.S.A.* **109**, 10210–10213 (2012).
28. R. Massart, E. Dubois, V. Cabuil, E. Hasmonay, *J. Magn. Magn. Mater.* **149**, 1–5 (1995).
29. D. Castelvecchi, *Phys. Rev. Focus* **15**, 18 (2005).
30. B. Berkovsky, V. Bashtovoi, *IEEE Trans. Magn.* **16**, 288–297 (1980).

Acknowledgments: We acknowledge financial support from the National Doctoral Programme in Materials Physics, Nokia Research Center, the Academy of Finland, a European Research Council Advanced Grant, and the Finnish Agency of Technology and Innovation (TEKES). Electron microscopy was performed using the devices of the Nanomicroscopy Center of Aalto University. We thank A. Walther (RWTH Aachen University), A. Kuzyk, and M. Kostiainen for comments on the manuscript and T. Huhtamäki and J. Korhonen for preparing the silicone nanofilament surfaces.

Supplementary Materials

www.sciencemag.org/cgi/content/full/341/6143/253/DC1
Materials and Methods
Supplementary Text
Figs. S1 to S10
References (*31*–*35*)
Movies S1 to S14

7 December 2012; accepted 10 June 2013
10.1126/science.1233775

Ultrahigh Magnetoresistance at Room Temperature in Molecular Wires

R. N. Mahato,[1] H. Lülf,[2] M. H. Siekman,[1,3] S. P. Kersten,[4] P. A. Bobbert,[4] M. P. de Jong,[1] L. De Cola,[2,5] W. G. van der Wiel[1]*

Systems featuring large magnetoresistance (MR) at room temperature and in small magnetic fields are attractive owing to their potential for applications in magnetic field sensing and data storage. Usually, the magnetic properties of materials are exploited to achieve large MR effects. Here, we report on an exceptionally large (>2000%), room-temperature, small-field (a few millitesla) MR effect in one-dimensional, nonmagnetic systems formed by molecular wires embedded in a zeolite host crystal. This ultrahigh MR effect is ascribed to spin blockade in one-dimensional electron transport. Its generic nature offers very good perspectives to exploit the effect in a wide range of low-dimensional systems.

In spintronic devices, the electron's spin is exploited for information processing. Typically, these devices contain layered structures with an electrical resistance that is dependent on the relative orientation of the magnetization of their magnetic layers; thus, the resistance can be altered by an external magnetic field, a phenomenon called magnetoresistance (MR). Examples include giant magnetoresistance (GMR) devices (*1*, *2*), which are multilayer stacks of ferromagnetic materials separated by a nonmagnetic metal spacer layer, and tunnel magnetoresistance (TMR) devices (*3*, *4*), which have a tunnel barrier as the spacer. Here, we explore entirely different physics in a nonmagnetic system, relying on a mechanism akin to spin blockade in quantum devices.

The Pauli principle precludes that an electron can tunnel into a state already occupied by another electron with the same spin. This spin blockade for two electrons starting from a spin-triplet configuration was first observed in quantum dots (QDs) at cryogenic temperatures (*5*). Spin blockade can be lifted by spin relaxation, mixing in singlet character. It has been shown that hyperfine interaction can lift spin blockade in QDs (*6*). The importance of hyperfine interaction on spin dynamics has also been recognized in the context of an intrinsic, room-temperature MR effect in organic semiconductors (*7*, *8*). Carrier transport is influenced by spin-dependent reactions, which are subject to the competition between an external magnetic field B and the random hyperfine fields B_{hf} (~1 mT) of the nuclei. At small B (Fig. 1A), hyperfine interactions

[1]NanoElectronics Group, MESA+ Institute for Nanotechnology, University of Twente, P.O. Box 217, 7500 AE, Enschede, Netherlands. [2]Institut de Science et d'Ingénierie Supramoléculaires (ISIS), Université de Strasbourg, 8 Allée Gaspard Monge, 67000 Strasbourg, France. [3]Transducers Science and Technology Group, MESA+ Institute for Nanotechnology, University of Twente, P.O. Box 217, 7500AE Enschede, Netherlands. [4]Theory of Polymers and Soft Matter, Department of Applied Physics, Eindhoven University of Technology, P.O. Box 513, 5600 MB, Eindhoven, Netherlands. [5]Karlsruher Institut für Technologie (KIT), Institut für Nanotechnologie Hermann-von-Helmholtz-Platz 1, D-76344 Eggenstein-Leopoldshafen, Germany.

*Corresponding author. E-mail: w.g.vanderwiel@utwente.nl

Retracted 9 October 2015; see first page.

mix in singlet character, hence lifting the blockade. However, at larger B, B_{hf} is overshadowed, so that spin blockade cannot be lifted (Fig. 1B). Unlike in QDs, spin blockade in organic molecules can occur at room temperature because of the much stronger wave function confinement, leading to a much larger energy spacing between the lowest singlet and triplet states.

In organic semiconductors exhibiting three-dimensional (3D) hopping conduction, the MR is rather small. It has been predicted, however, that confinement of the current path in molecular systems could lead to a strong increase of the MR (*9*). Here, we realize such a system experimentally. Our system (Fig. 2) consists of strictly 1D wires, formed by subliming organic dye molecules, DXP (N,N′-bis(2,6-dimethylphenyl)-perylene-3,4,9,10-tetracarboxylic diimide), into the channels of zeolite L crystals in the presence of potassium as counterion of its alumina sites (*10*). Zeolite L is a well-known, electrically insulating aluminosilicate crystalline system (*11*), which consists of many thousands of separated channels with a maximum diameter of 1.26 nm, running through the whole crystal and oriented perfectly parallel to the cylinder c axis. The geometrical constraints of the zeolite host structure allow for the formation of 1D chains of highly uniaxially oriented, closely spaced molecules. The 2.2-nm-long DXP molecules only fit into a channel in their length direction. Although DXP's rigid van der Waals width is ~0.76 nm, DXP can be inserted into the 0.71-nm channel opening above ~175°C (*12*). We used relatively small size zeolites (30- to 100-nm height; 200- to 500-nm diameter), enabling an 86% DXP loading degree (*10*). At these high filling ratios, (hopping) electron transport along molecular wires can be readily observed in our conducting-probe atomic force microscopy (CP-AFM) experiments, making this system suitable for 1D transport measurements. DXP-loaded zeolites have been applied before as artificial photonic antenna systems (*11*), where energy transfer occurs due to near-field interaction. A number of studies report on the electrical conductivity of zeolites loaded with metal atoms (*13*, *14*) or conductive polymers (*15*, *16*), as well as on the effect of inserting different charge-balancing cations (*17*–*19*). However, most of this work focuses on bulk systems of a large number of randomly oriented zeolites, with the exception of (*20*).

Magnetotransport measurements were carried out on DXP-loaded zeolites on top of an ITO|PEDOT:PSS [indium tin oxide|poly(3,4-ethylenedioxythiophene):poly(styrenesulfonate)] substrate at room temperature in an ultrahigh vacuum CP-AFM with a PtSi tip. We estimate that ~10^2 channels contribute in parallel to electron transport (*10*). The measurements were obtained from zeolites with heights of 30, 45, 60, 80, and 90 nm. For every height, the results were reproduced for at least two different zeolites. The current (I)–voltage (V) characteristics in Fig. 3 are almost symmetric in voltage, in accordance

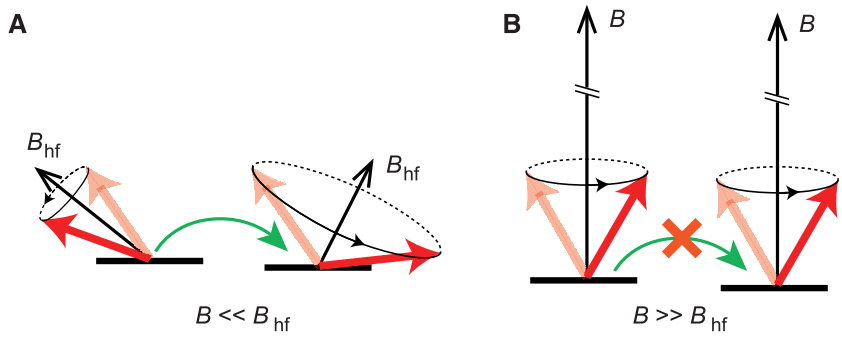

Fig. 1. Magnetic field dependence of spin blockade. Shaded (unshaded) arrows indicate an initial (final) spin configuration at neighboring sites before (after) spin precession. (**A**) For $B << B_{hf}$, spin blockade can be lifted due to spin mixing induced by hyperfine interaction. (**B**) If $B >> B_{hf}$, spin mixing is suppressed and spin blockade can occur.

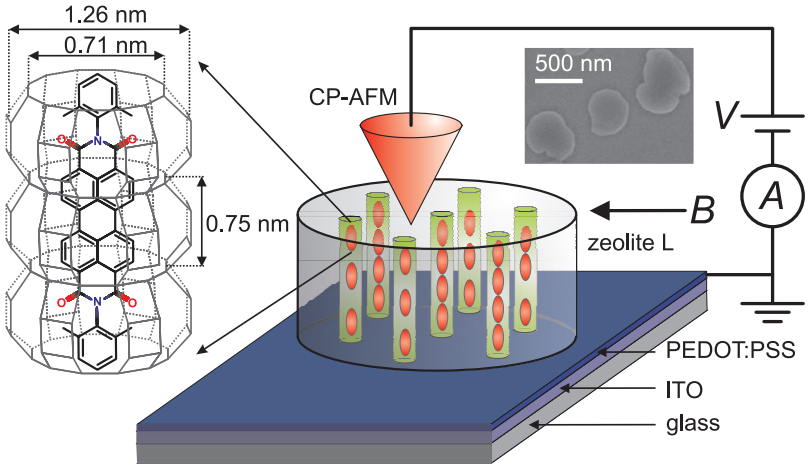

Fig. 2. Measurement setup and sample structure. The CP-AFM measures the conduction of the molecules (red ellipsoids) aligned in zeolites on ITO|PEDOT:PSS. (**Left**) Zeolite channel with a DXP molecule inside. (**Upper right**) Scanning electron micrograph of zeolites.

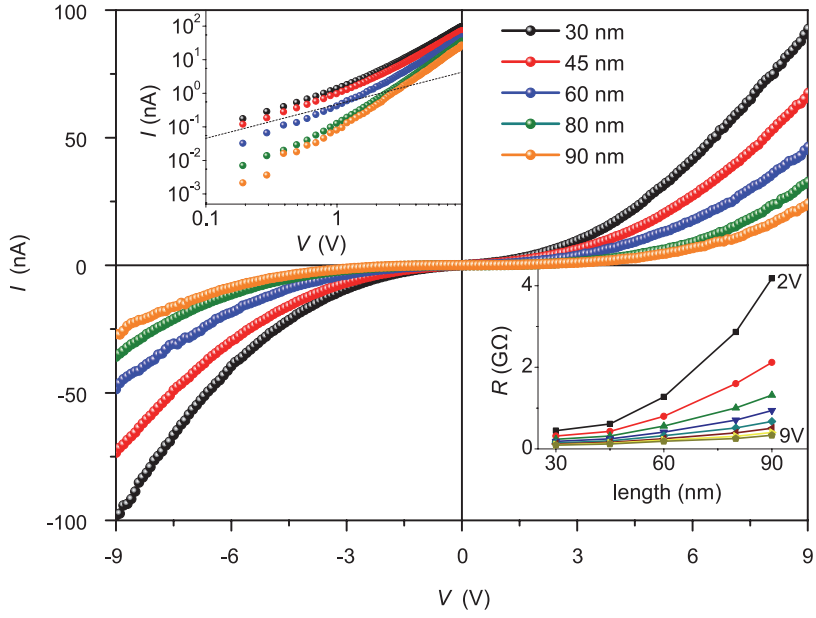

Fig. 3. Electrical characterization of DXP-loaded zeolites. Room-temperature I-V characteristics for different channel length. (**Upper left inset**) Same data on log-log scale. The straight dashed line indicates a linear dependence. (**Lower right inset**) Resistance $R = V/I$ versus channel length.

with the similarity of the work functions of the two contacts. The *I-V* characteristics are typical for energetically disordered systems with hopping transport. The upper left inset displays the same data on a logarithmic *I* scale, showing a transition from a linear behavior (indicated by the dashed line) at low voltage to a superlinear power-law behavior at high voltage. The resistance, $R = V/I$, as a function of channel length for different voltages, is given in the lower right inset. The increase of the resistance with length changes from exponential at low voltage to linear at higher voltages. As the resistance is dependent on channel length, the conductivity is limited by the molecular wires rather than by the contacts. The symmetric *I-V* curves and absence of an injection barrier indicate unipolar transport. Both PEDOT:PSS and PtSi have work functions around –5 eV (*21*, *22*), roughly in the middle between the energies of the highest occupied and lowest unoccupied molecular orbital (HOMO and LUMO) of DXP (–6.0 and –3.9 eV, respectively) (*23*). This seems to be at odds with the absence of an injection barrier. However, the mobile potassium ions in the channels could substantially change the injection barrier by creating dipole layers at the zeolite surface, lowering the barrier for electron injection. This would be consistent with electron transport (see below), but our considerations would be equally valid for hole transport. The linear regime in the *I-V* curves points at the presence of free charges, and hence free spins, in the channels already at low voltage. These should result from diffusion from the contacts (PEDOT:PSS layer and PtSi tip) into the interior of the zeolite, yielding an exponentially decaying charge concentration profile compatible with the observed exponential dependence of the resistance on channel length at low voltage. We confirmed that empty zeolites do not show any detectable current up to 9 V. Likewise, CP-AFM measurements on ITO|PEDOT:PSS substrates give linear *I-V*s with negligible resistance (*10*).

Figure 4A shows the current-voltage characteristic for a 60-nm channel length at zero magnetic field and at 14 mT perpendicular to the wires, plotting $|I|$ on a logarithmic scale. Despite the small magnetic field, a very strong current suppression is observed at 14 mT, especially at lower voltage. To study the magnetic field dependence of the current through the molecular wires in more detail, we define the magnetoconductance (MC) as

$$\mathrm{MC}(B) \equiv \frac{I(B) - I(0)}{I(0)} \qquad (1)$$

where $I(B)$ is the current at magnetic field B, and $I(0)$ the current at zero magnetic field, yielding a maximum possible negative MC of –100%. Figure 4B shows MC(B) at different bias voltages for a 60-nm wire length. We observe a very large, negative MC, monotonically increasing with decreasing voltage. Similar behavior was observed for other wire lengths (*10*).

The MC(B) curves can be fitted well with the empirical line shape

$$\mathrm{MC}(B) \propto \frac{B^2}{(B_0 + |B|)^2} \qquad (2)$$

applied before in the context of organic magnetoresistance (OMAR) (*7*). It has a characteristic width B_0, related to the magnitude of the hyperfine fields. The fitted B_0 values (fig. S2) vary between 2 and 6 mT, comparable to values obtained for OMAR (*7*), and show almost no voltage dependence. The mT field scale agrees well with the typical hyperfine coupling in π-conjugated molecules, clearly pointing at a molecular origin. The very large room-temperature MC approaching the maximum possible value of –100% is notable.

The voltage dependence is more clearly represented if we convert MC to the more common MR, defined by

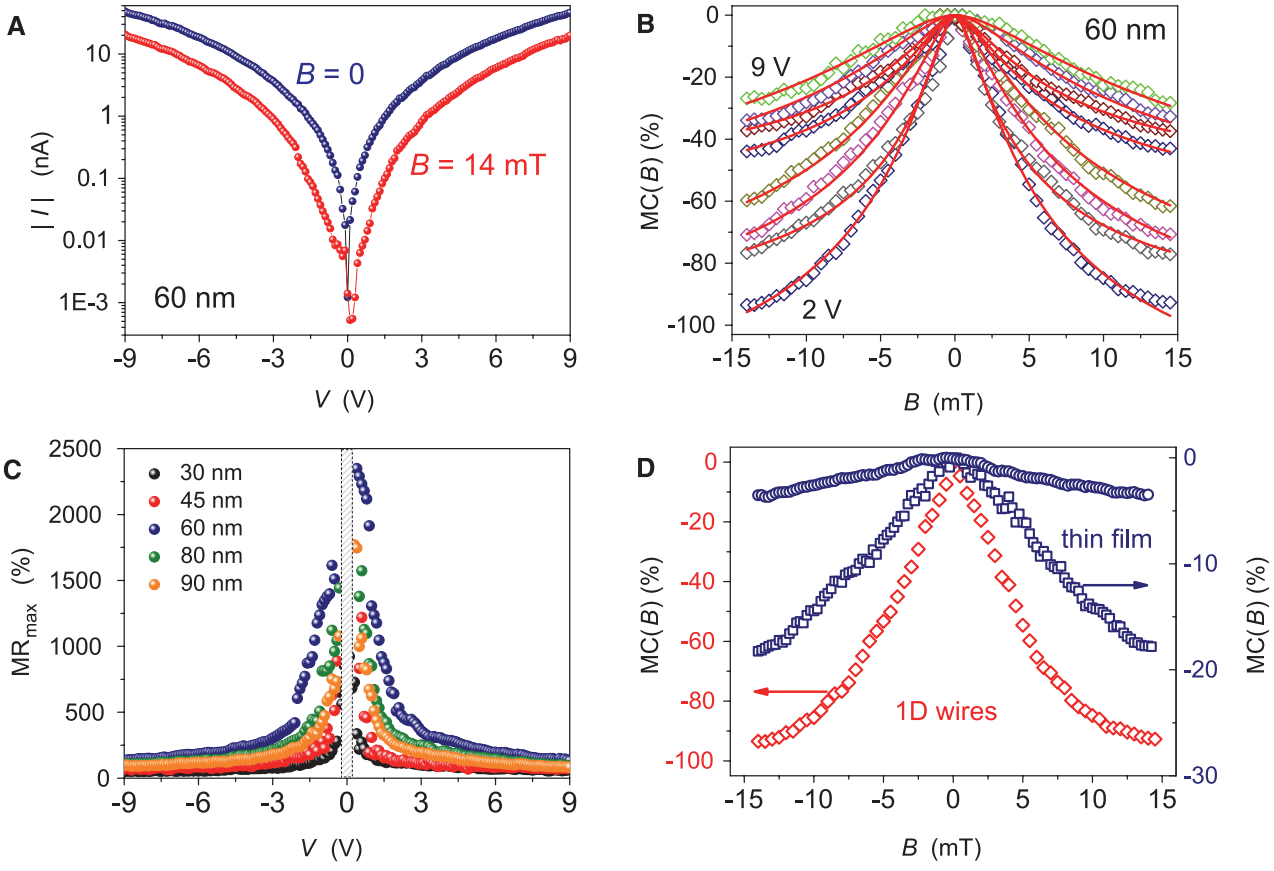

Fig. 4. Room-temperature MR. (**A**) *I-V* characteristics of DXP-loaded zeolite with 60-nm channel length at $B = 0$ and 14 mT. (**B**) Magnetoconductance MC(B) at different bias voltages for 60-nm channel length. The red curves are fits to Eq. 2. (**C**) Maximum magnetoresistance $\mathrm{MR}_{max} = [R(B_{max}) - R(0)]/R(0)$, as a function of V for different channel lengths. (**D**) Comparison between MC in a ~40-nm DXP film measured by a 250-μm-diameter Pt wire (blue circles), the same film measured by a CP-AFM PtSi tip (blue squares), and 60-nm-long 1D DXP wires measured by a PtSi CP-AFM tip (red diamonds).

Retracted 9 October 2015; see first page.

$$\mathrm{MR}(B) \equiv \frac{R(B) - R(0)}{R(0)} = \frac{I(0) - I(B)}{I(B)} \quad (3)$$

where $R(B)$ is the resistance at magnetic field B and $R(0)$ the resistance at zero field. We have derived $MR_{max}(V)$ from the I-Vs for different channel lengths at zero magnetic field and maximum magnetic field, B_{max}, according to $MR_{max}(V) = [I(V,0) - I(V,B_{max})]/I(V,B_{max})$, (Fig. 4C). The MR increases rapidly with decreasing voltage, reaching a maximum value of more than 2000% for 60-nm wire length when approaching 0 V. Because the current levels are below the noise limit close to 0 V, we have not been able to determine MR_{max} here.

The MR values in our molecular wires compare favorably with values reported for other systems under similar conditions. The highest room-temperature TMR value reported to date is 600% for an epitaxial CoFeB/MgO/CoFeB magnetic tunnel junction (*24*). Collosal magnetoresistance (CMR) manganites exhibit very large low-temperature MR at several tesla (*25*); however, room-temperature, low-field MR values are a few tens of percents (*26*, *27*). For nanocomposites containing magnetic nanoparticles, MR values similar to those in CMR experiments have been demonstrated under comparable experimental conditions (*28*). A large room-temperature MR effect of a few tens of percents was also reported for a graphene nanoribbon field-effect transistor (*29*).

We ascribe our very large MR values to the unique 1D character of our system. Indeed, nonstructured DXP thin films show much lower MR values (Fig. 4D). When a ~40-nm DXP film is contacted with a PtSi CP-AFM tip in the same setup, we measure a maximum MC of around –20%. With a Pt wire of 250-μm diameter instead of the PtSi tip, the maximum MC is reduced to about –5%. These results strongly suggest that confinement of the current path is crucial for explaining our results, in line with recent numerical studies (*9*). Explanations based on spin-dependent interactions involving excited states (*30*, *31*) can be ruled out, because the MR is also present—and even more pronounced—below the DXP HOMO-LUMO gap (~2 eV). The fact that for DXP the energy required to form doubly negatively charged states is remarkably small [~0.2 eV from cyclic voltammetry measurements (*23*)] suggests that such states are involved in transport. We therefore propose that the current is carried by electrons and that spin blockade is caused by two electrons residing on neighboring molecules attempting to form a doubly negatively charged molecule in a spin-singlet configuration by hopping of one of the electrons. The energetic disorder generally present in organic systems facilitates formation of doubly charged molecules at favorable locations. Moreover, the presence of a positively charged potassium ion close to a DXP molecule strongly reduces its LUMO level, also facilitating double charging. Simulations show that with these ingredients, MC values close to –100% indeed can be obtained with MC (B) curves having the line shape of Eq. 2 (*10*). Further analysis should provide more insight into the details of the mechanism behind the effect, but the present experimental results clearly point at spin blockade tuned by a competition between the external magnetic field and the random internal hyperfine field.

References and Notes

1. M. N. Baibich *et al.*, *Phys. Rev. Lett.* **61**, 2472–2475 (1988).
2. G. Binasch, P. Grünberg, F. Saurenbach, W. Zinn, *Phys. Rev. B* **39**, 4828–4830 (1989).
3. M. Jullière, *Phys. Lett.* **54**, 225–226 (1975).
4. J. S. Moodera, L. R. Kinder, T. M. Wong, R. Meservey, *Phys. Rev. Lett.* **74**, 3273–3276 (1995).
5. K. Ono, D. G. Austing, Y. Tokura, S. Tarucha, *Science* **297**, 1313–1317 (2002).
6. R. Hanson, L. P. Kouwenhoven, J. R. Petta, S. Tarucha, L. M. K. Vandersypen, *Rev. Mod. Phys.* **79**, 1455–1455 (2007).
7. T. Francis, Ö. Mermer, G. Veeraraghavan, M. Wohlgenannt, *New J. Phys.* **6**, 185 (2004).
8. W. Wagemans *et al.*, *Spin* **1**, 93–108 (2011).
9. S. P. Kersten, S. Meskers, P. A. Bobbert, *Phys. Rev. B* **86**, 045210 (2012).
10. Materials and methods are available as supplementary materials on *Science* Online.
11. G. Calzaferri, S. Huber, H. Maas, C. Minkowski, *Angew. Chem. Int. Ed.* **42**, 3732–3758 (2003).
12. P. Bornhauser, G. Calzaferri, *J. Phys. Chem.* **100**, 2035–2044 (1996).
13. P. A. Anderson *et al.*, *Dalton Trans.* **19**, 3122–3128 (2004) and references therein.
14. M. J. Kelly, *J. Phys. Condens. Matter* **7**, 5507–5519 (1995).
15. T. Bein, in *Recent Advances and New Horizons in Zeolite Science and Technology*, H. Chon, S. I. Woo, S. E. Park, Eds. (Elsevier, Amsterdam, 1996), pp. 295–322.
16. D. J. Cardin, *Adv. Mater.* **14**, 553 (2002).
17. U. Simon, M. E. Franke, in *Host-Guest-Systems Based on Nanoporous Crystals*, F. Laeri, F. Schüth, U. Simon, M. Wark, Eds. (Wiley, Weinheim, 2003), pp. 364–378.
18. M. Álvaro *et al.*, *Chem. Mater.* **18**, 26–33 (2006).
19. F. J. Jansen, R. A. Schoonheydt, *J. Chem. Soc., Faraday Trans.* **69**, 1338 (1973).
20. Z. K. Tang *et al.*, *Science* **292**, 2462 (2001).
21. A. M. Nardes *et al.*, *Org. Electron.* **9**, 727–734 (2008).
22. H. Bentmann, A. A. Demkov, R. Gregory, S. Zollner, *Phys. Rev. B* **78**, 205302 (2008).
23. S. K. Lee *et al.*, *J. Am. Chem. Soc.* **121**, 3513–3520 (1999).
24. S. Ikeda *et al.*, *Appl. Phys. Lett.* **93**, 082508 (2008).
25. G. Q. Gong *et al.*, *Appl. Phys. Lett.* **67**, 1783 (1995).
26. P. K. Siwach, H. K. Singh, O. N. Srivastava, *J. Phys. Condens. Matter* **20**, 273201 (2008).
27. Y.-T. Zhang, Z.-Y. Chen, C.-C. Wang, Q. Jie, H.-B. Lü, *J. Magn. Magn. Mater.* **321**, 1199–1201 (2009).
28. F. J. Yue *et al.*, *J. Phys. D Appl. Phys.* **44**, 025001 (2011).
29. J. Bai *et al.*, *Nat. Nanotechnol.* **5**, 655–659 (2010).
30. V. N. Prigodin, J. D. Bergeson, D. M. Lincoln, A. J. Epstein, *Synth. Met.* **156**, 757–761 (2006).
31. P. Desai, P. Shakya, T. Kreouzis, W. P. Gillin, *Phys. Rev. B* **76**, 235202 (2007).

Acknowledgments: We thank B. Koopmans, L. Abelmann, L. P. Kouwenhoven, Y. Tokura, and S. Tarucha for fruitful discussions. We acknowledge financial support from the Netherlands Technology Foundation STW, the European Research Council, ERC Starting Grant nos. 240433 and 280020, ERC Advanced Grant no. 247365, NanoScience Europe program (NanoSci-ERA), grant no. 11003, and the Foundation for Fundamental Research on Matter (FOM), part of the Netherlands Organisation for Scientific Research (NWO). A link to the data reported here is included in the supplementary materials. R.N.M. and M.H.S. carried out the magnetoresistance experiments and performed the data analysis. H.L. performed the zeolite L crystal synthesis and molecular loading. W.G.v.d.W. conceived the experiments and planned and supervised the project. L.D.C. conceived the project together with W.G.v.d.W. and supervised the zeolite synthesis and loading. S.P.K. and P.A.B. performed the theoretical analysis and numerical simulations. M.P.d.J. contributed to planning and supervision. All authors discussed the results, provided important insights, and helped write the manuscript.

Supplementary Materials

www.sciencemag.org/cgi/content/full/science.1237242/DC1
Materials and Methods
Figs. S1 to S4
Data Files
References (*32*–*37*)

1 March 2013; accepted 14 June 2013
Published online 4 July 2013;
10.1126/science.1237242

Isotope Ratios of H, C, and O in CO_2 and H_2O of the Martian Atmosphere

Chris R. Webster,[1]* Paul R. Mahaffy,[2] Gregory J. Flesch,[1] Paul B. Niles,[6] John H. Jones,[7] Laurie A. Leshin,[3] Sushil K. Atreya,[4] Jennifer C. Stern,[2] Lance E. Christensen,[1] Tobias Owen,[5] Heather Franz,[2] Robert O. Pepin,[8] Andrew Steele,[9] the MSL Science Team†

Stable isotope ratios of H, C, and O are powerful indicators of a wide variety of planetary geophysical processes, and for Mars they reveal the record of loss of its atmosphere and subsequent interactions with its surface such as carbonate formation. We report in situ measurements of the isotopic ratios of D/H and $^{18}O/^{16}O$ in water and $^{13}C/^{12}C$, $^{18}O/^{16}O$, $^{17}O/^{16}O$, and $^{13}C^{18}O/^{12}C^{16}O$ in carbon dioxide, made in the martian atmosphere at Gale Crater from the Curiosity rover using the Sample Analysis at Mars (SAM)'s tunable laser spectrometer (TLS). Comparison between our measurements in the modern atmosphere and those of martian meteorites such as ALH 84001 implies that the martian reservoirs of CO_2 and H_2O were largely established ~4 billion years ago, but that atmospheric loss or surface interaction may be still ongoing.

The Sample Analysis at Mars (SAM) suite (*1*) on the Curiosity rover that landed in August 2012 is conducting a search for organic compounds and volatiles in rocks and soils and characterizing the chemical and isotopic composition of the modern atmosphere. Atmo-

Ultrahigh Magnetoresistance at Room Temperature in Molecular Wires

R. N. Mahato *et al.*

Science **341**, 257 (2013);
DOI: 10.1126/science.1237242